

Chapter 4

Low Dimensional Magnetism:

A Ru(III)-Ni(II) Cyano Bridged 1-D Coordination Polymer

Adapted from:

Duimstra, J.A., Stern, C.L., Meade, T.J. (2006) *Polyhedron*, accepted

Introduction

Chapter 3 detailed the progress toward a ruthenium-gadolinium dyad complex designed to modulate the electronic relaxation time of gadolinium(III). This complex was based upon Ru(III) coordinated by a salen-derived ligand. Through the course of the investigations, a cyanide bridged Ru(III)-Ru(III) complex was discovered (Figure 3-4), indicating that the cyanide ligand could function as an effective bridge between Ru(III) metal centers. This observation led to research into low dimensional magnetic materials based on the $\text{Ru}(\text{salen})(\text{CN})_2^-$ building block.

Low dimensional metal-based coordination polymers have attracted recent attention due to unique magnetic properties of these compounds such as slow relaxation and quantum tunneling of the magnetization.^[1] 3-D magnets typically show a magnetic phase transition at a critical temperature, T_c , below which the individual magnetic moments are aligned with respect to each other. The alignment can be either ferromagnetic where the moments are all in the same direction, or anti-ferromagnetic with the moments aligning in alternate directions. The alignment is confined to a given region known as a domain. The critical temperature in a 3-D material can be readily assessed using heat capacity measurements. When the material undergoes magnetic ordering, the phase transition is apparent in a plot of the heat capacity as a function of temperature and gives rise to a spike known as a λ -peak.^[2]

In a low dimensional magnetic material the metal ions are isolated magnetically from each other in one or more spatial directions while retaining magnetic coupling in the remaining dimensions. Hence a bulk phase transition at T_c does not occur in these systems. Instead, the anisotropy of the material can instill a slow relaxation of the

magnetization below a critical temperature known as the blocking temperature, T_{block} .^[3-5] Thus the material behaves as a magnet below T_{block} and is referred to as a single molecule magnet (SMM) or a single chain magnet (SCM) if it is either a zero dimensional cluster or a one dimensional chain respectively. The small size of low dimensional magnets makes them attractive targets for high density data storage. In this application the size of a bit of data is anticipated to be smaller than the domain size of a comparable bit in a 3-D material.

In order for a material to display slow relaxation of the magnetization or 3-D magnetic ordering, the material must behave as a magnet. The temperature range in which the material behaves as a magnet may be determined by measuring the zero-field cooled (zfc) and field-cooled (fc) magnetization of the material. In this experiment the sample is cooled in zero applied field. An external dc magnetic field that does not saturate the sample is then applied and the magnetization is measured as the sample is allowed to warm. This is the zfc portion of the experiment. In the fc measurement, the sample is cooled in the applied field while the magnetization is measured. The magnetization as a function of temperature is then plotted for both the zfc and the fc segments of the experiment. If the sample shows magnetic behavior the zfc and fc curves will diverge at the critical or blocking temperature. At temperatures below the divergence point the sample displays the irreversible behavior characteristic of a magnet.

After determination of the temperature range where the material displays bulk magnetic behavior, the magnetic relaxation properties of the material may be examined. The presence of slow relaxation of the magnetization can be ascertained through measuring the frequency dependence of the ac magnetic susceptibility near the blocking

temperature.^[6, 7] In this experiment the sample is subjected to a small alternating magnetic field in the absence of an applied static (or dc) magnetic field. The moments of the material then attempt to align with the alternating field as it changes. The inductive response of the sample is measured as a function of temperature at a given applied ac frequency and consists of in-phase (real) and out-of-phase (imaginary) susceptibilities. The experiment is repeated several times at different ac frequencies. If the relaxation of the magnetization of the material is slow, the moments will not be able to respond quickly to the applied ac field and the out-of-phase susceptibility will vary as a function of applied ac frequency.^[2] This variation can be fit to the Arrhenius equation to give an energy barrier for magnetization relaxation. Materials that display 3-D magnetic ordering do not display this frequency dependent behavior. Thus, the presence of a frequency dependent out-of-phase ac magnetic susceptibility is a hallmark of SCMs and SMMs.

Compounds that display slow relaxation of their magnetization typically consist of paramagnetic metal ions bridged by a small coordinating ligand such as azide, oxalate or cyanide. Examples of azide bridged coordination polymers include $[\text{Co}(2,2'\text{-bithiazoline})(\text{N}_3)_2]_n$, a 1-D polymer that displays single-chain magnetic behavior with a blocking temperature of 5 K,^[5] while a large class of 2-D coordination polymers based on the oxalate (ox) ligand has also been investigated. The oxalate compounds have the general formula $[\text{M}(\text{II})\text{M}'(\text{III})(\text{ox})_3]^-$ where M is a 3d ion such as Mn, Fe, Co or Cu and $\text{M}' = \text{Cr}^{[8, 9]}$ or $\text{Fe}^{[10]}$. These compounds display a range of magnetic behavior depending on the different metals and cations involved.

The cyanide ligand plays an important design role in the field of low dimensional magnetic coordination polymers as it effectively bridges two metal centers in a

predictable linear arrangement.^[11, 12] A cyanide-bridged 1-D single chain magnet comprised of Fe(III) and Co(II) ions arranged in a zigzag fashion displayed slow relaxation of the magnetization below 8 K,^[13] and superparamagnetic behavior has been observed in a cyanide-bridged Fe(III)₂Cu(II) coordination polymer.^[14]

Incorporation of paramagnetic 4d ions into low dimensional coordination polymers is intriguing due to the more covalent metal-ligand bonds and increased spin-orbit coupling present in the second transition row metals compared to the 3d ions. Several studies have focused on molybdenum(III). Long and coworkers have used Mo(III)(Me₃tacn)(CN)₃ (Me₃tacn is N,N',N''-trimethyl-1,4,7-triazacyclononane) to produce clusters of Mo(III) magnetically coupled to Ni(II) ions.^[15] These clusters show higher magnetic anisotropy and better orbital overlap compared with the analogous compounds containing Cr(III) substituted for Mo(III). Other examples such as 2-D K₂Mn(II)₃(H₂O)₆[Mo(III)(CN)₇]₂•6H₂O have used Mo(III)(CN)₇⁴⁻ as a building block.^[16]

Examples of low dimensional ruthenium(III) based polymers are rare however, having been limited until very recently^[17] to M(II)Ru(III)oxalato complexes (M is a 3d ion) that typically adopt a 2-D network.^[18, 19] Initially the sign of the exchange coupling in the M(II)Ru(III)oxalato complex (M = Cu(II)) was thought to not obey simple symmetry considerations,^[18] but an alternative interpretation showed that the interaction does indeed conform to symmetry-based expectations.^[19]

Results and Discussion

Synthesis and structural characterization

Chapter 3 detailed research using the (3,3'-bismethoxy)salen' ligand and it was

from this ligand that the Ru(III)-Ru(III) dimer was derived. The methoxy groups were present for chelation of Gd(III) and chelated a sodium counterion effectively in $\text{Na}[\text{Ru}(\text{III})(3,3'\text{-bismethoxy})\text{salen}'(\text{CN})_2]$. However, the presence of these additional chelating groups was anticipated to cause unwanted complications in the study of materials designed to focus on the metal-metal bridging ability of the cyanide ligand. Therefore, the underivatized salen ligand was used for the studies in this chapter.

Formation of $\text{Ru}(\text{III})\text{salen}(\text{PPh}_3)\text{Cl}$, **1**, was achieved via initial ligand complexation of the Ru(II) compound, $\text{Ru}(\text{II})(\text{PPh}_3)_3\text{Cl}_2$, forming a red, presumably $\text{Ru}(\text{II})\text{salen}(\text{PPh}_3)_2$, complex. The Ru(II) compound was then oxidized in ethanol using air to generate **1**. This method is preferred over the literature method^[20] of simultaneous complexation and oxidation as it reduces oxidized byproducts. Single crystals suitable for X-ray diffraction of compound **1** were grown from vapor diffusion of diethyl ether into a methanolic solution of the compound. The structure is depicted in Figure 4-1 with crystallographic data and selected bond lengths and angles given in Tables 4-2 and 4-3, respectively. Comparison with $\text{Ru}(\text{III})(3,3'\text{-bismethoxy})\text{salen}'(\text{PPh}_3)\text{Cl}$ (see Chapter 3) shows that the bond lengths are all slightly longer for **1**, in line with the lower electron donating ability of the underivatized salen ligand compared to the methoxy substituted ligand used in Chapter 3.

The cyanide complex, $\text{Na}[\text{Ru}(\text{III})\text{salen}(\text{CN})_2]$, **2** was prepared by refluxing **1** in MeOH with sodium cyanide.^[21] Passage of the crude material through an alumina plug followed by recrystallization via vapor diffusion of ether into methanol generated pure compound. Crystals of **2** suitable for X-ray diffraction were grown from slow evaporation of a methanolic solution (Tables 4-3 and 4-4 and Figure 4-2). Due to the

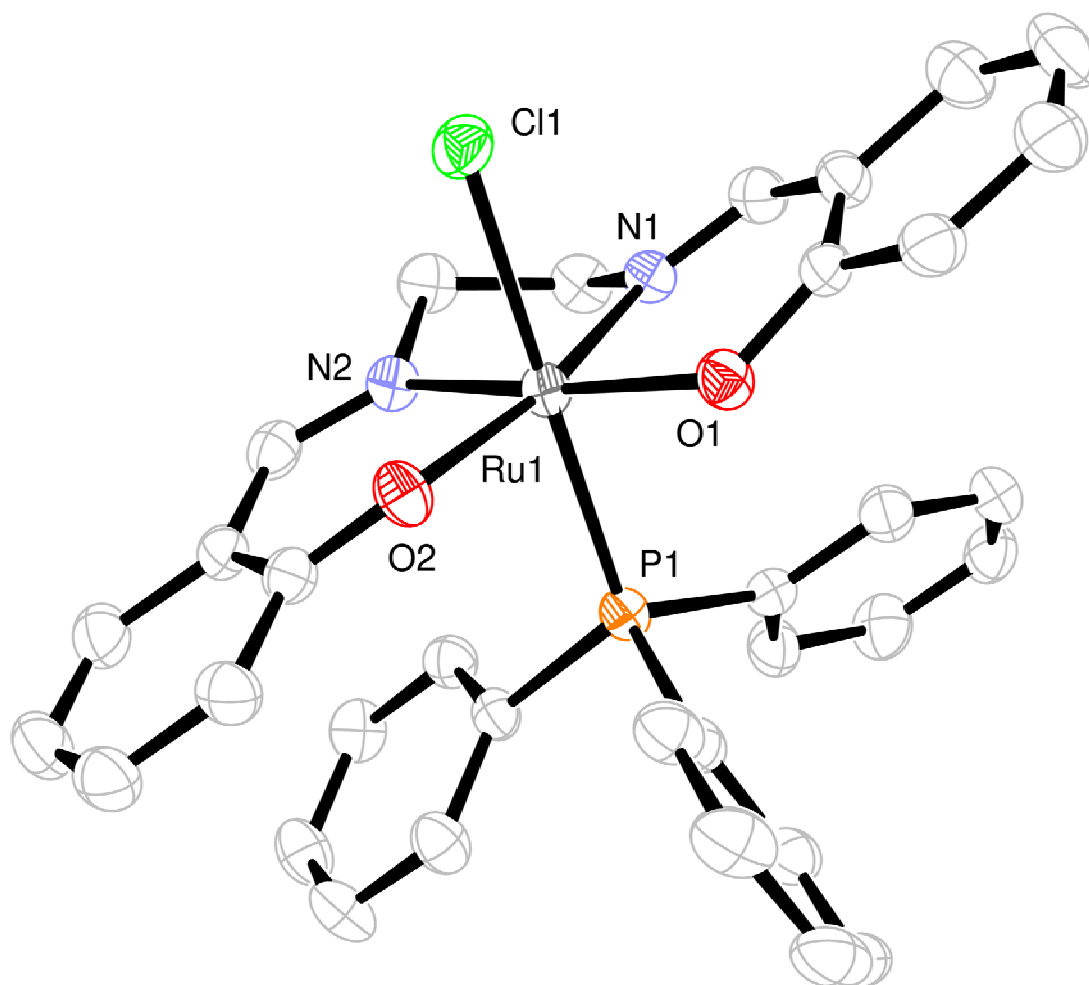


Figure 4-1: Thermal ellipsoid (50%) depiction of Ru(III)salen(PPh₃)Cl, **1**. Hydrogen atoms have been removed for clarity.

Table 4-1: Crystallographic details for **1**.

1	
Empirical formula	C ₃₄ H ₂₉ N ₂ ClO ₂ PRu
Formula weight	665.08
Crystal system	Monoclinic
Space group	<i>P2₁/c</i>
<i>a</i> (Å)	11.033(2)
<i>b</i> (Å)	21.079(3)
<i>c</i> (Å)	12.665(2)
β (°)	101.101(17)
<i>V</i> (Å ³)	2890.2(8)
<i>Z</i>	4
ρ (calc) (g cm ⁻³)	1.528
μ (mm ⁻¹)	0.725
Reflections collected/unique	27788/7283 [$R_{\text{int}} = 0.0671$]
Data/restraints/parameters	7283/0/370
Goodness-of-fit on F^2	0.919
Final <i>R</i> indices [$I > 2(\sigma)I$]	$R_1 = 0.0318$, $wR_2 = 0.0640$
<i>R</i> indices (all data)	$R_1 = 0.0551$, $wR_2 = 0.0679$

Table 4-2: Selected bond lengths (Å) and angles (°) for compound **1**.

Ru(1)-N(1)	1.9881(17)
Ru(1)-O(1)	2.0156(14)
Ru(1)-N(2)	2.0020(17)
Ru(1)-O(2)	2.0260(15)
Ru(1)-P(1)	2.3747(7)
Ru(1)-Cl(1)	2.4410(6)
P(1)-Ru(1)-Cl(1)	178.10(2)
N(1)-Ru(1)-N(2)	82.63(7)
N(1)-Ru(1)-O(1)	90.70(7)
N(1)-Ru(1)-O(2)	170.92(6)

lack of coordinating methoxy groups on the salen ligand the sodium counterion is not bound within the ligand framework as it was for $\text{Na}[\text{Ru}(\text{III})(3,3'\text{-bismethoxy)salen}'(\text{CN})_2]$ (Chapter 3). Instead, the sodium counterion interacts with cyanide atom N3# from one adjacent Ru(III) complex (at $1-x, -1/2+y, 1/2-z$) and cyanide N4# from another nearby Ru(III) complex (at $1+x, y, z$) giving rise to a 2-D layered structure (Figure 4-3). As a result, the C17-Ru1-C18 angle is $172.88(7)^\circ$ while Ru1-C17-N3 and Ru1-C18-N4 display angles of $170.45(16)^\circ$ and $172.18(16)^\circ$, respectively. The coordination sphere of sodium is completed by salen oxygens O1 and O2 and a methanol solvent molecule. Comparison with *trans*-NBu₄[Ru(III)(salen)(CN)₂]^[17] shows the significant distortion arising from the sodium counterion. As a tetrabutylammonium salt, there is no interaction between Ru(III) centers resulting in nearly linear angles for C17-Ru1-C18 ($178.3(7)^\circ$), Ru1-C17-N3 ($178(1)^\circ$) and Ru1-C18-N4 ($176(1)^\circ$).^[17] The Ru-C and C≡N bond lengths for **2** fall within the range observed by Yeung et al.

Reaction of equimolar Ni(II)(cyclam) perchlorate^[22] in solvents such as water, acetone and acetonitrile with **2** in water resulted in immediate precipitation of a fine steel blue particulate of formulation [Ru(III)(salen)(CN)₂][Ni(II)(cyclam)](ClO₄) (**3**). X-ray quality needles of **3** resulted from slow diffusion of Ni(II)(cyclam)(ClO₄)₂ in acetonitrile into an aqueous solution of **2** (Tables 4-3 and 4-5, Figure 4-3). The C≡N stretching frequency shifts to higher energy from 2099 cm^{-1} in **2** to 2126 cm^{-1} in **3**, with concomitant bond shortening of the cyano moiety from $1.153(2)\text{ \AA}$ for N3-C17 and $1.150(2)\text{ \AA}$ for N4-C18 in **2** to $1.135(6)\text{ \AA}$ and $1.144(5)\text{ \AA}$, respectively, in compound **3**. These results are comparable to that seen by Yeung et al. upon addition of NiCl₂ and cyclam to $\text{Ru}(\text{acac})_2(\text{CN})_2^-$ and are consistent with N coordination to the Ni(cyclam)

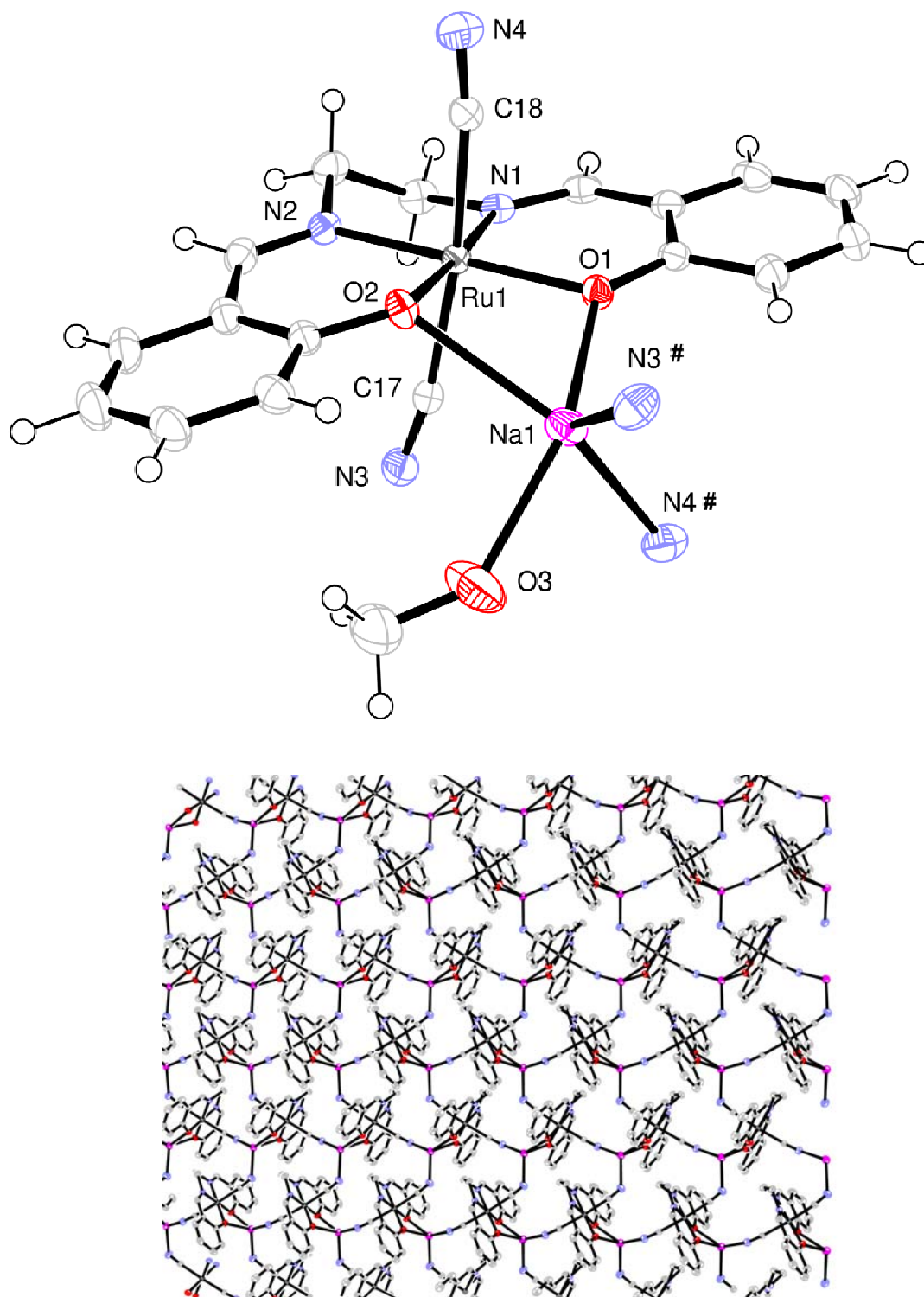


Figure 4-2: Thermal ellipsoid (50%) plot of **2•MeOH** (top). View of 2-D plane of **2•MeOH** with MeOH solvates and hydrogen atoms removed for clarity (bottom).

Table 4-3: Crystallographic data for **2** and **3**.

	2 •MeOH	3 •H ₂ O•MeCN
Empirical formula	C ₁₉ H ₁₈ N ₄ NaO ₃ Ru	C ₃₀ H ₄₃ ClN ₉ NiO ₇ Ru
Formula weight	474.43	836.93
Crystal system	Monoclinic	Triclinic
Space group	<i>P2</i> ₁ / <i>c</i>	<i>P</i> $\bar{1}$
<i>a</i> (Å)	7.3220(9)	9.6253(11)
<i>b</i> (Å)	12.4263(16)	14.2047(17)
<i>c</i> (Å)	20.662(3)	20.662(3)
α (°)	90	94.109(2)
β (°)	92.362(2)	99.171(2)
γ (°)	90	107.940(2)
<i>V</i> (Å ³)	1878.3(4)	1816.1(4)
<i>Z</i>	4	2
ρ (calc) (g cm ⁻³)	1.674	1.520
μ (mm ⁻¹)	0.886	1.064
Reflections collected/unique	17596/4667 [<i>R</i> _{int} = 0.0411]	16822/8465 [<i>R</i> _{int} = 0.0381]
Data/restraints/parameters	4667/0/254	8465/0/446
Goodness-of-fit on <i>F</i> ²	1.072	1.098
Final <i>R</i> indices [<i>I</i> > 2(σ)]	<i>R</i> ₁ = 0.0235, <i>wR</i> ₂ = 0.0608	<i>R</i> ₁ = 0.0612, <i>wR</i> ₂ = 0.1584
<i>R</i> indices (all data)	<i>R</i> ₁ = 0.0286, <i>wR</i> ₂ = 0.0624	<i>R</i> ₁ = 0.0843, <i>wR</i> ₂ = 0.1793

Table 4-4: Selected bond lengths (Å) and angles (°) for compound **2**•MeOH.

Ru(1)-N(2)	1.9818(14)	Na(1)-O(1)	2.3104(13)
Ru(1)-N(1)	1.9844(14)	Na(1)-O(3)	2.3621(18)
Ru(1)-O(2)	2.0305(12)	Na(1)-N(3)#	2.4162(19)
Ru(1)-O(1)	2.0159(12)	Na(1)-N(4)#	2.4916(18)
Ru(1)-C(17)	2.0745(18)	Na(1)-O(2)	2.6157(15)
Ru(1)-C(18)	2.0773(18)	N(3)-C(17)	1.153(2)
Ru(1)-Na(1)	3.2777(8)	N(4)-C(18)	1.150(2)
N(3)-C(17)-Ru(1)	170.45(16)	N(4)-C(18)-Ru(1)	172.18(16)
Ru(1)-O(2)-Na(1)	88.81(5)	C(17)-Ru(1)-C(18)	172.88(7)

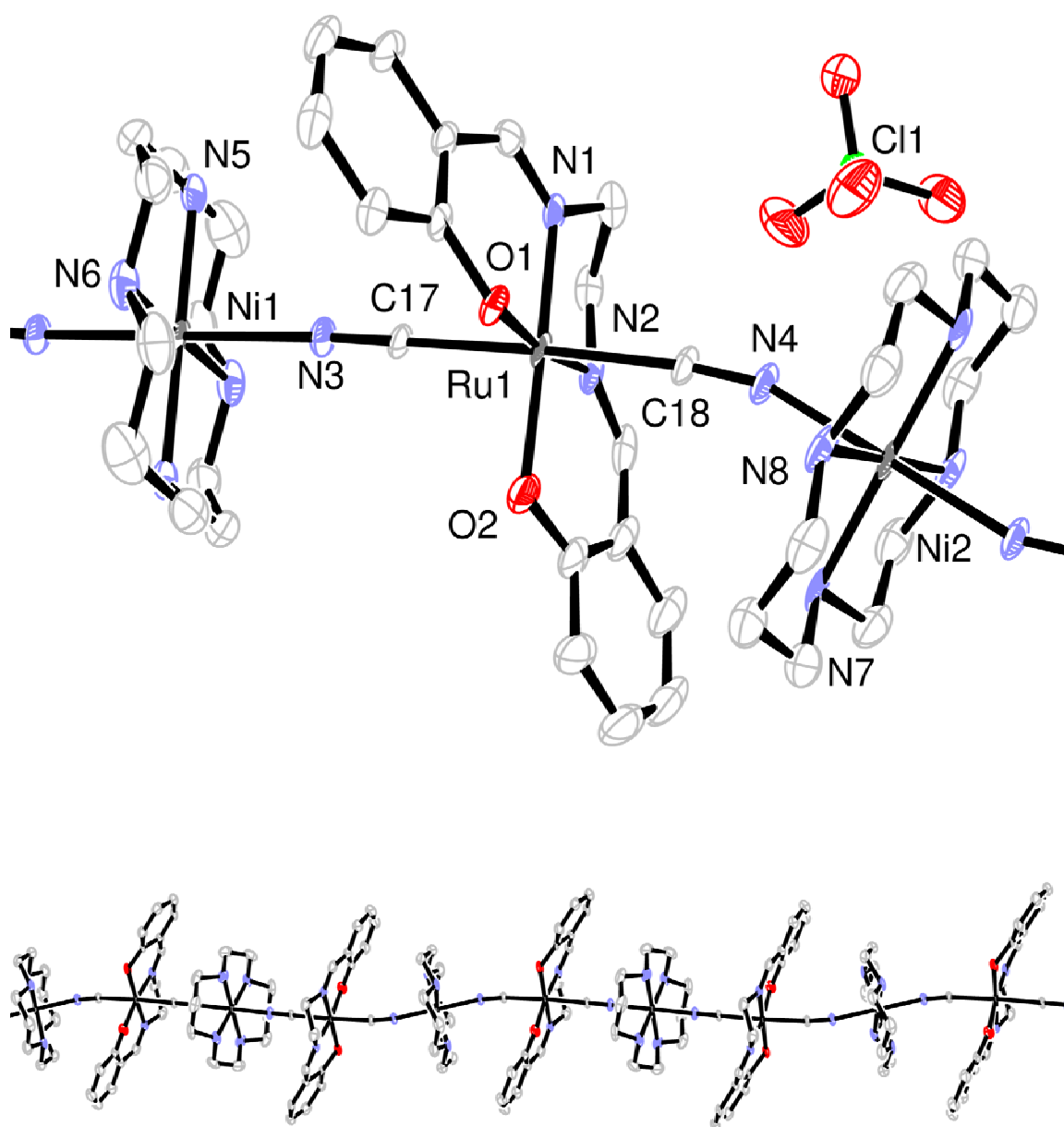


Figure 4-3: Thermal ellipsoid plot (50%) of [Ru(III)(salen)(CN)₂]

[Ni(II)(cyclam)](ClO₄)·H₂O·MeCN (**3**·H₂O·MeCN) (top). Water and MeCN solvates and hydrogen atoms have been removed for clarity. View of cationic portion of **3**·H₂O·MeCN perpendicular to crystallographic *a* axis showing several repeat units (bottom).

Table 4-5: Selected bond lengths (Å) and angles (°) for compound **1**•MeCN•H₂O.

Ru(1)-N(2)	1.994(4)	Ni(1)-N(5)	2.068(4)
Ru(1)-N(1)	2.001(3)	Ni(1)-N(6)	2.075(4)
Ru(1)-O(2)	2.016(3)	Ni(1)-N(3)	2.080(4)
Ru(1)-O(1)	2.026(3)	Ni(2)-N(8)	2.057(4)
Ru(1)-C(17)	2.058(4)	Ni(2)-N(7)	2.072(4)
Ru(1)-C(18)	2.072(4)	Ni(2)-N(4)	2.134(4)
N(3)-C(17)	1.135(6)	N(4)-C(18)	1.144(5)
N(2)-Ru(1)-N(1)	171.97(14)	N(3)-C(17)-Ru(1)	179.6(4)
N(2)-Ru(1)-O(1)	89.79(13)	N(4)-C(18)-Ru(1)	173.5(4)
N(1)-Ru(1)-O(1)	90.96(15)	C(17)-Ru(1)-C(18)	177.14(16)
N(2)-Ru(1)-O(2)	172.45(14)		
N(1)-Ru(1)-O(2)	96.78(13)	N(5)-Ni(1)-N(6)	94.62(16)
O(1)-Ru(1)-O(2)	92.16(15)	N(5)-Ni(1)-N(3)	89.61(14)
N(2)-Ru(1)-C(17)	86.98(14)	N(6)-Ni(1)-N(3)	89.73(15)
N(1)-Ru(1)-C(17)	90.09(14)	N(8)-Ni(2)-N(7)	85.78(17)
O(1)-Ru(1)-C(17)	89.27(14)	N(8)-Ni(2)-N(4)	87.14(15)
O(2)-Ru(1)-C(17)	86.91(15)	N(7)-Ni(2)-N(4)	91.67(14)
N(2)-Ru(1)-C(18)	95.58(16)	C(17)-N(3)-Ni(1)	175.6(4)
N(1)-Ru(1)-C(18)	91.19(14)	C(18)-N(4)-Ni(2)	159.9(4)
O(1)-Ru(1)-C(18)	88.04(15)		
O(2)-Ru(1)-C(18)	171.97(14)		

subunit. The Ru1-C17 distance in **3** is 2.058(4) Å while Ru1-C18 is similar to that in **2** at 2.072(4) Å. Around Ni, the Ni1-N3 distance is 2.080(4) Å while Ni2-N4 is 2.134(4) Å. With the exception of Ni2-N4, these distances are identical to those reported for the trimeric Ni(cyclam)[Ru(acac)₂(CN)₂]₂.^[17] For **3**, the aromatic rings on the salens of adjacent chains stack with an average separation of 3.31 Å.

The presence of the perchlorate anion results in a deviation from linearity of the -(Ru-CN-Ni-NC)- fragment giving rise to two different Ni(II) sites. The two Ni atoms lie on independent inversion centers. Along the metal cyanide axis, the Ni1 site is nearly linear with an angle of 175.6(4)° between Ni1-N3-C17 and an angle of 179.6(4)° between N3-C17-Ru1. The analogous measurements around Ni2 display a more bent shape with 159.9(4)° for Ni2-N4-C18 and 173.5(4)° between N4-C18-Ru1.

Magnetic properties

The results of temperature dependent magnetic susceptibility measurements performed on powder samples of compounds **2** and **3** in a field of 1 kOe are shown in Figure 4-4. At room temperature $\chi_M T$ for **2** is 0.51 cm³ mol⁻¹ K, considerably higher than the calculated spin-only value of 0.38 cm³ mol⁻¹ K for $S = 1/2$, but comparable to other monomeric Ru(III) complexes such as *trans*-Ph₄P[Ru(III)(acac)₂(CN)₂]^[23] and Ru(III)(acac)₃.^[24] The shape of the curve closely resembles that observed for *trans*-Ph₄P[Ru(III)(acac)₂(CN)₂] and polymeric [CoCp₂*][ZnRu(ox)₃]^[18] all of which display a gradual decrease in $\chi_M T$ from 300 K to approximately 15 K with a subsequent steep drop below 15 K. Correction for a temperature independent paramagnetism (TIP) contribution of 5 x 10⁻⁴ cm³ mol⁻¹ renders $\chi_M T$ independent of temperature from 300 K to 100 K with a

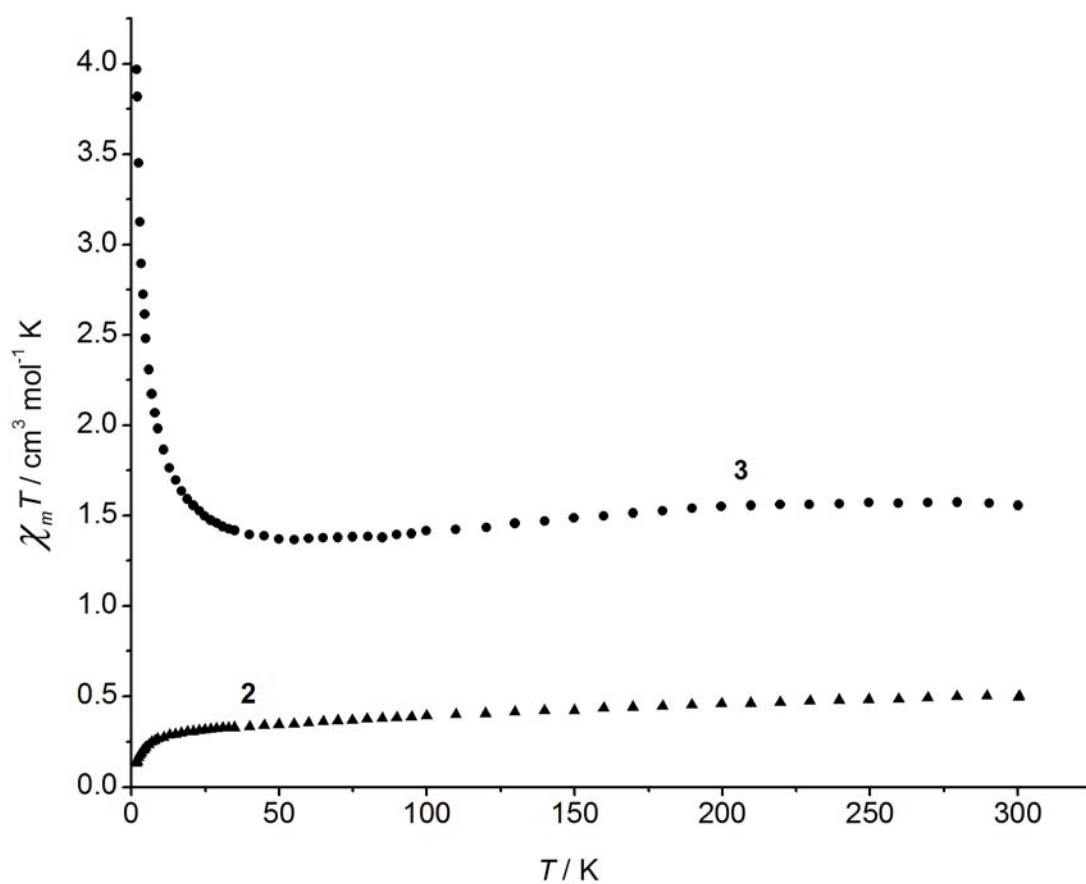


Figure 4-4: Magnetic susceptibility as a function of temperature for compounds **2** and **3** in the range of 2-300 K at an applied field of 1 kOe. TIP correction is not included.

value of $0.36 \text{ cm}^3 \text{ mol}^{-1} \text{ K}$ in agreement with the spin only value. As noted by Coronado et al.,^[18] the low temperature behavior below 15 K arises from spin-orbit coupling and incomplete quenching of the orbital contribution to the magnetic moment and can cause difficulties in the interpretation of susceptibility data containing Ru(III) ions as seen below.

For chain **3**, $\chi_M T$ is $1.57 \text{ cm}^3 \text{ mol}^{-1} \text{ K}$ at 300 K, higher than the calculated spin only value of $1.38 \text{ cm}^3 \text{ mol}^{-1} \text{ K}$ for uncorrelated $S=1$ Ni(II) and $S=1/2$ Ru(III) ions, but in good agreement with the calculated result of $1.51 \text{ cm}^3 \text{ mol}^{-1} \text{ K}$ using the data obtained for **2**. Applying the same TIP correction used in the analysis of **2** gives a $\chi_M T$ of $1.42 \text{ cm}^3 \text{ mol}^{-1} \text{ K}$ at 300 K but does not remove the minimum at 55 K. The presence of the minimum would seem to indicate an antiferromagnetic interaction between Ru(III) and Ni(II). This conclusion was drawn from similar data by Kahn and coworkers for the 2-D $(\text{NBu}_4)[\text{Cu(II)Ru(III)(ox)}_3]$ framework.^[19] An alternative interpretation that appears to be more applicable in this case attributes the minimum to the anisotropic Ru(III) ion and indicates that the type of coupling must be determined through examination of the low temperature field-dependent magnetization data.^[18]

The magnetization of **3** as a function of applied field at 2 K is depicted in Figure 4-5. At 50 kOe, the magnetization is nearly saturated with a value of $2.46 \mu_B$. The magnetization may be calculated using the Brillouin function for a given spin quantum number.^[2] The calculated curves at 2 K and a g value of 2 are depicted in Figure 4-5 for $S = 1/2$ and $S = 3/2$. At high applied fields the magnetization tends toward a saturation value. The calculated saturation magnetization (M_s) for a spin-only system consisting of ferromagnetically coupled Ni(II) ($S = 1$) and Ru(III) ($S = 1/2$) is $3 \mu_B$. Antiferromagnetic

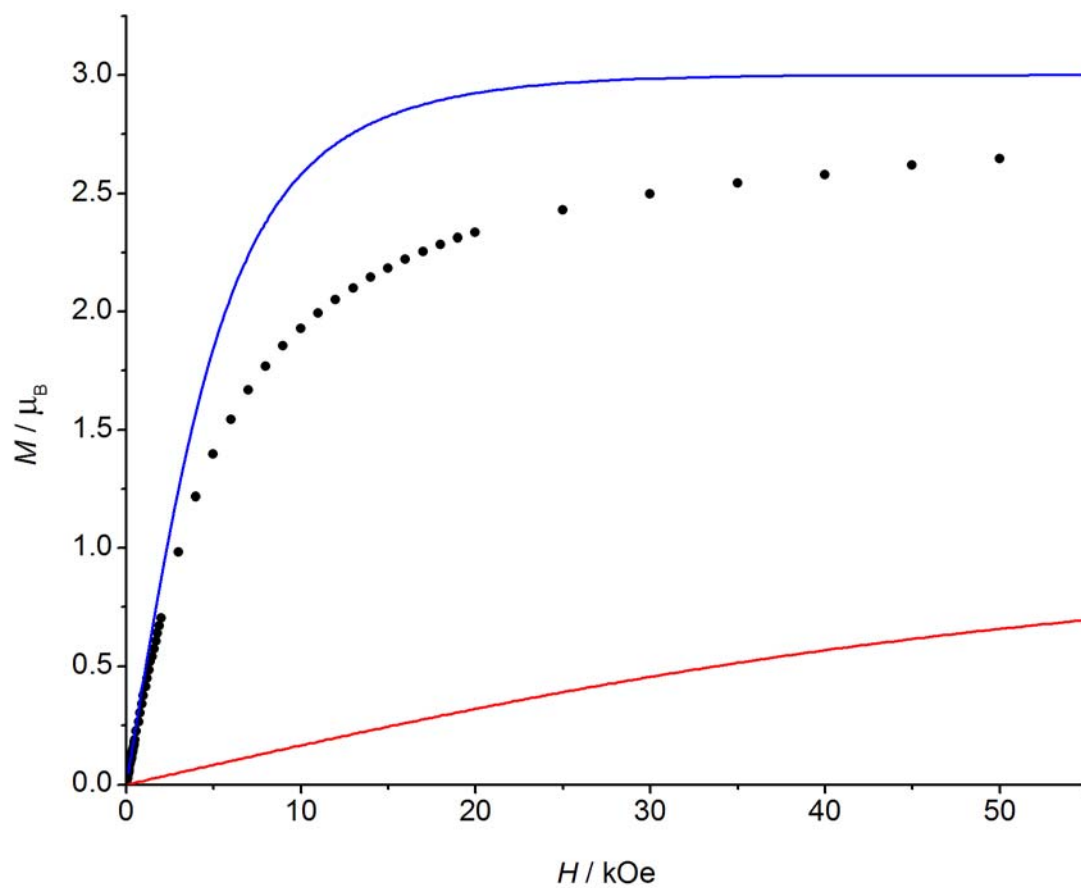


Figure 4-5: Magnetization of **3** as a function of applied field at 2.0 K. The red line is the calculated magnetization for $S = 1/2$ while the blue line is the calculated curve for $S = 3/2$.

coupling of the two ions results in a calculated M_s of $1 \mu_B$. The experimentally observed value clearly indicates ferromagnetic coupling, a conclusion that agrees with the results of Coronado et al. and with the expected orthogonality of magnetic orbitals between Ni(II) and Ru(III).^[17, 18] The lower than expected saturation value can be attributed to the Ru(III) ion.^[18, 24]

Zero-field cooled (zfc) and field-cooled (fc) magnetization experiments performed on **3** in applied fields of 3 and 50 Oe show no inflection point and little difference down to 3 K (Figure 4-6). These measurements indicate a lack of any type of long-range magnetic order above 3 K. Further evidence for the absence of 3-D ordering above 2 K is given by the lack of a λ -peak in the heat capacity measurements (Figure 4-7) of **3** indicating that there is no magnetic phase transition. Compound **3** displays negligible hysteresis at 2 K.

Conclusion

Although **3** does not display slow relaxation of the magnetization above 3 K, the salen ligand is readily amenable to synthetic modification that could be used to affect the magnetism of the compound through changes in the electronics at the Ru(III) center. It is interesting to note that a similar species, Ni(cyclam)[Ru(acac)₂(CN)₂]₂, is trimeric,^[17] reflecting the marked effect small structural changes can have on the dimensionality of the resulting mixed metal system. The current results demonstrate that Ru(III) can be incorporated into a 1-D coordination polymer and provide further evidence that simple symmetry considerations can be used to predict whether the ion will display a ferro- or antiferromagnetic exchange interaction.

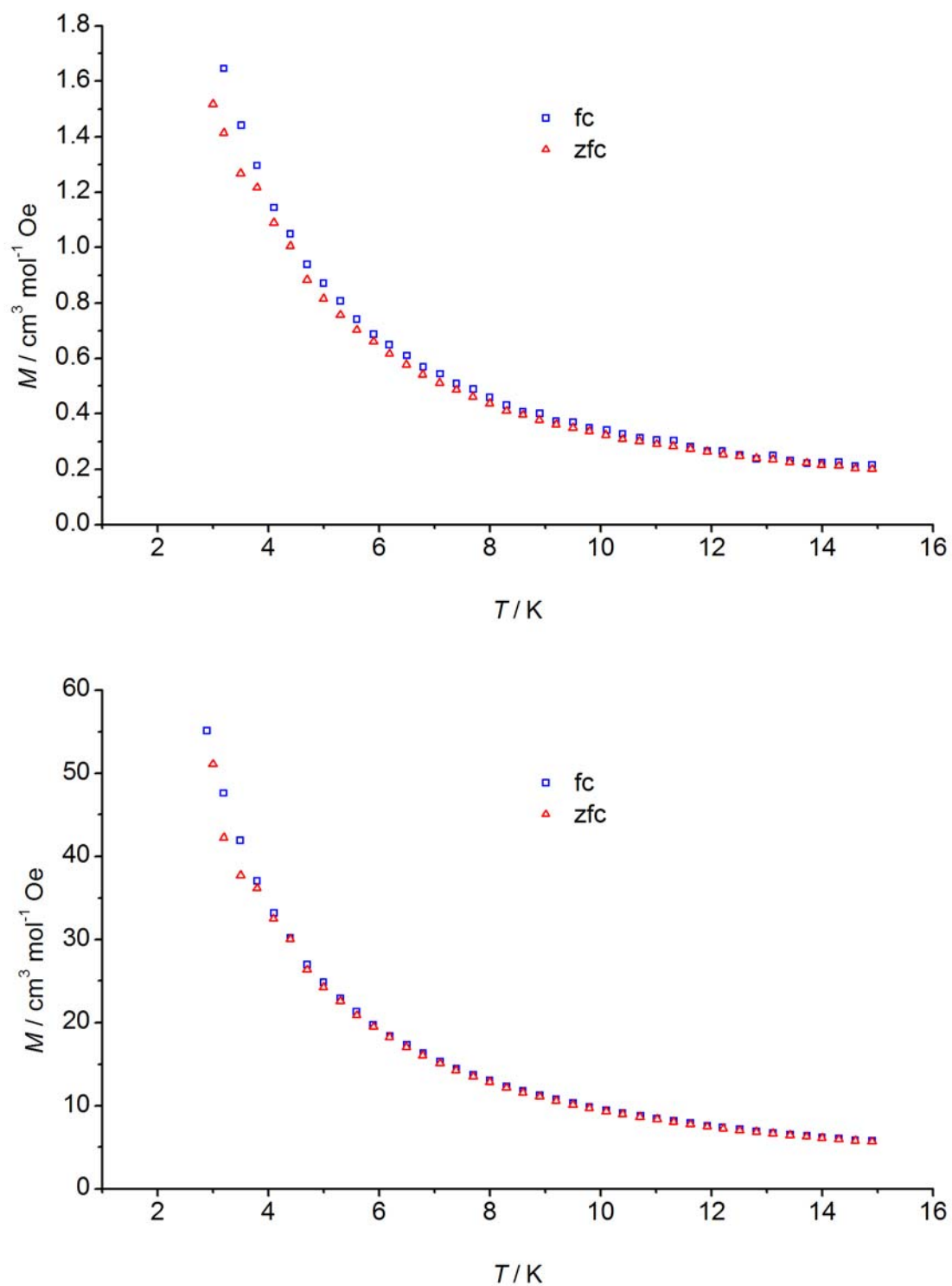


Figure 4-6: Zero-field cooled (zfc) and field-cooled (fc) magnetization of compound **3** at an applied field of 3 Oe (top) and 50 Oe (bottom).

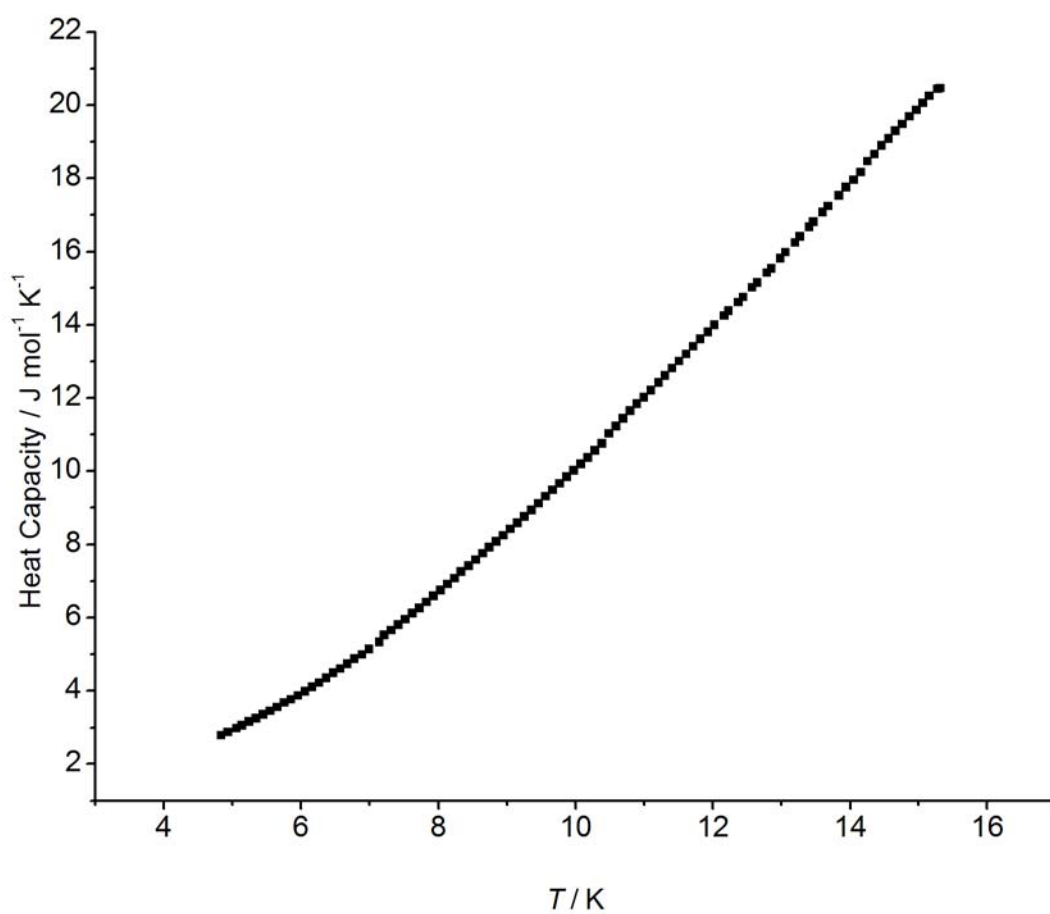


Figure 4-7: Heat capacity of compound **3**. The line is smooth and shows no λ - peak, indicating 3-D magnetic ordering does not occur above 2 K.

Experimental

General Methods:

[Ni(cyclam)](ClO₄)₂ was prepared according to the literature procedure.^[22] Mass spectra were obtained by infusing a methanolic solution of the compound into a Varian 1200L single quadrupole mass spectrometer. Infrared spectra of KBr pellets were recorded using a Biorad FTS-60 FTIR spectrometer. Elemental analyses were performed by Desert Analytics (Tucson, AZ). Variable temperature magnetic susceptibility and heat capacity measurements were performed by Dr. Oleksandr Chernyashevskyy of the Materials Research Science and Engineering Center at Northwestern University. The magnetic measurements were taken of powder samples on a Quantum Design MPMS SQUID magnetometer in the temperature range of 2-300 K. Susceptibilities were corrected for the sample holder and the diamagnetism of the sample calculated from Pascal's constants. Heat capacity measurements were performed in zero applied field on a Quantum Design PPMS.

Ru(III)salen(PPh₃)Cl: (1)^[20]

Salen (1.40 g, 5.23 mmol) and triethylamine (2.91 mL, 20.9 mmol) were refluxed in ethanol (125 mL) for 45 min, at which point the reaction was cooled and Ru(PPh₃)₃Cl₂ (5.01 g, 5.23 mmol) was added. The suspension was heated and allowed to remain at reflux until all solid material had been consumed (3.5 h), generating a deep red solution. The solution was allowed to cool while a stream of air was bubbled through the reaction for 1.5 h. The solution was filtered through Celite and concentrated to ~ 5 mL. Diethyl ether (200 mL) was added and the mixture was cooled to -20 °C. The solids were collected by filtration after 1 day and recrystallized from THF (70 mL initially,

concentrated to 50 mL). This procedure yielded 2.50 g (72%) of compound **1**. X-ray quality crystals were obtained upon vapor diffusion of diethyl ether into a methanolic solution of the compound. ESI-MS m/z (MeOH) (M-Cl⁻) appropriate isotope pattern, maximum at 630.1 (100%); Anal. Calcd for C₃₄H₂₉ClN₂O₂PRu: C 61.40, H 4.39, N 4.21; Found: C 61.44, H 4.22, N 4.54.

Na[Ru(III)salen(CN)₂]: (2)^[21]

In methanol (125 mL) were combined Ru(III)salen(PPh₃)Cl, **1**, (2.44 g, 3.67 mmol) and sodium cyanide (396 mg, 8.07 mmol). The solution was refluxed for 1 h and concentrated *in vacuo*. The crude material was purified by chromatography (1:1 methylene chloride : methanol; neutral alumina) and recrystallized by slow vapor diffusion of diethyl ether into a methanol solution of the compound. This yielded 700 mg (43%) of compound **2**. Blue crystalline plates suitable for X-ray diffraction were grown from slow evaporation of a methanolic solution. IR (KBr pellet) $\nu_{\text{CN}} = 2099 \text{ cm}^{-1}$. MS (ESI) m/z (M - Na⁺) appropriate isotope pattern, maximum at 420.1. Anal. for C₁₈H₁₄N₄NaO₂Ru•1.5H₂O Calcd.: C, 46.06; H, 3.65; N, 11.94; Found: C, 46.04; H, 3.64; N, 11.67.

[Ru(III)(salen)(CN)₂][Ni(II)(cyclam)](ClO₄): (3)

[Ni(cyclam)](ClO₄)₂ (104 mg; 0.226 mmol) in acetonitrile (5 mL) was added dropwise to a solution of **2** (100 mg, 0.226 mmol) in water (5 mL). The resulting blue precipitate was isolated by centrifugation, washed with water and acetonitrile and dried *in vacuo* yielding 126 mg **3** (72%). Blue needle-like crystals of **3** suitable for X-ray diffraction resulted from slow diffusion of Ni(II)(cyclam)(ClO₄)₂ in acetonitrile into an aqueous solution of **2**. IR (KBr pellet) $\nu_{\text{CN}} = 2126 \text{ cm}^{-1}$. Anal. for C₂₈H₃₈ClN₈NiO₆Ru

Calcd.: C, 43.23; H, 4.92; N, 14.41. Found: C, 43.39; H, 5.11; N, 14.09.

X-ray Crystallography:

The crystallographic data were collected and solved by Dr. Charlotte Stern of the Analytical Services Laboratory at Northwestern University. The data were collected on a Bruker SMART 1000 X-ray diffractometer with CCD detector using graphite monochromated Mo K α radiation ($\lambda = 0.71073 \text{ \AA}$). Data sets for **1**, **2** and **3** were obtained at 153(2) K. For **1** data were collected within a theta range of 1.88 to 29.32° in 0.3° oscillations with 15 s exposures. For **2** the data were collected with a theta range of 1.91 to 29.12°. Data were obtained in 0.3° oscillations with 10 s exposures. For **3**, the theta range for data collection was 1.46 to 28.65° and data were collected in 0.3° oscillations with 25 s exposures. The crystal-to-detector distance was 50.00 mm with the detector at the 28° swing position for all compounds. Data were processed using SAINT-NT from Bruker and were corrected for Lorentz and polarization effects. The structures were solved by direct methods,^[25] expanded using Fourier techniques and refined by full matrix least squares on F^2 .^[26] The non-hydrogen atoms were refined anisotropically. Hydrogen atoms were included in idealized positions but not refined with the exception of the hydroxyl hydrogen in the methanol solvate of **2** and the hydrogen atoms of the water solvent molecule in **3**. These H-atoms could not be located in reasonable positions. Crystallographic data for **1** and **2** are tabulated in Table 4-1 with selected bond lengths and angles given in Tables 4-2 and 4-3 for **1** and **2**, respectively. Crystallographic data for **3** is given in Table 4-4 and selected bond lengths and angles are listed in Table 4-5.

References

- [1] Coronado, E., Palacio, F., Veciana, J. (2003) Molecule-based magnetic materials. *Angewandte Chemie, International Edition in English*, **42**: 2570-2572.
- [2] Itoh, K., Kinoshita, M.: Molecular magnetism: New magnetic materials. Kodansha; Gordon and Breach, Tokyo; Amsterdam 2000.
- [3] Miyasaka, H., Clérac, R. (2005) Synthetic strategy for rational design of single-chain magnets. *Bulletin of the Chemical Society of Japan*, **78**: 1725-1748.
- [4] Clérac, R., Miyasaka, H., Yamashita, M., Coulon, C. (2002) Evidence for single-chain magnet behavior in a Mn(III)-Ni(II) chain designed with high spin magnetic units: A route to high temperature metastable magnets. *Journal of the American Chemical Society*, **124**: 12837-12844.
- [5] Liu, T.-F., Fu, D., Gao, S., Zhang, Y.-Z., Sun, H.-L., Su, G., Liu, Y.-J. (2003) An azide-bridged homospin single-chain magnet: $[\text{Co}(2,2'\text{-bithiazoline})(\text{N}_3)_2]_n$. *Journal of the American Chemical Society*, **125**: 13976-13977.
- [6] Caneschi, A., Gatteschi, D., Lalioti, N., Sangregorio, C., Sessoli, R., Venturi, G., Vindigni, A., Rettori, A., Pini, M.G., Novak, M.A. (2001) Cobalt(II)-nitronyl nitroxide chains as molecular magnetic nanowires. *Angewandte Chemie, International Edition in English*, **40**: 1760-1763.
- [7] Lescouëzec, R., Vaissermann, J., Ruiz-Pérez, C., Lloret, F., Carrasco, R., Julve, M., Verdager, M., Dromzee, Y., Gatteschi, D., Wernsdorfer, W. (2003) Cyanide-bridged iron(III)-cobalt(II) double zigzag ferromagnetic chains: Two new molecular magnetic nanowires. *Angewandte Chemie, International Edition in English*, **42**: 1483-1486.
- [8] Tamaki, H., Zhong, Z.J., Matsumoto, N., Kida, S., Koikawa, M., Achiwa, N., Hashimoto, Y., Okawa, H. (1992) Design of metal-complex magnets. Syntheses and magnetic properties of mixed-metal assemblies $\{\text{NBu}_4[\text{MCr}(\text{ox})_3]\}_x$ (NBu_4^+ = tetra(n-butyl)ammonium ion; ox^{2-} = oxalate ion; $\text{M} = \text{Mn}^{2+}, \text{Fe}^{2+}, \text{Co}^{2+}, \text{Ni}^{2+}, \text{Cu}^{2+}, \text{Zn}^{2+}$). *Journal of the American Chemical Society*, **114**: 6974-6979.
- [9] Decurtins, S., Schmalle, H.W., Oswald, H.R., Linden, A., Ensling, J., Gütllich, P., Hauser, A. (1994) A polymeric two-dimensional mixed-metal network. Crystal structure and magnetic properties of $\{[\text{P}(\text{Ph})_4][\text{MnCr}(\text{ox})_3]\}_n$. *Inorganica Chimica Acta*, **216**: 65-73.
- [10] Decurtins, S., Schmalle, H.W., Schneuwly, P., Pellaux, R., Ensling, J. (1995) Polymeric two- and three-dimensional transition-metal networks. Crystal structures and magnetic properties. *Molecular Crystals and Liquid Crystals*

Science and Technology, Section A: Molecular Crystals and Liquid Crystals, **273**: 605-612.

- [11] Beltran, L.M.C., Long, J.R. (2005) Directed assembly of metal-cyanide cluster magnets. *Accounts of Chemical Research*, **38**: 325-334.
- [12] Dunbar, K.R., Heintz, R.A. (1997) Chemistry of transition metal cyanide compounds: Modern perspectives. *Progress in Inorganic Chemistry*, **45**: 283-391.
- [13] Toma, L.M., Lescouëzec, R., Lloret, F., Julve, M., Vaissermann, J., Verdaguer, M. (2003) Cyanide-bridged Fe(III)-Co(II) bis double zigzag chains with a slow relaxation of the magnetisation. *Chemical Communications*: 1850-1851.
- [14] Wang, S., Zuo, J.-L., Gao, S., Song, Y., Zhou, H.-C., Zhang, Y.-Z., You, X.-Z. (2004) The observation of superparamagnetic behavior in molecular nanowires. *Journal of the American Chemical Society*, **126**: 8900-8901.
- [15] Shores, M.P., Sokol, J.J., Long, J.R. (2002) Nickel(II)-molybdenum(III)-cyanide clusters: Synthesis and magnetic behavior of species incorporating $[(\text{Me}_3\text{tacn})\text{Mo}(\text{CN})_3]$. *Journal of the American Chemical Society*, **124**: 2279-2292.
- [16] Larionova, J., Kahn, O., Gohlen, S., Ouahab, L., Clérac, R. (1999) Structure, ferromagnetic ordering, anisotropy, and spin reorientation for the two-dimensional cyano-bridged bimetallic compound $\text{K}_2\text{Mn}_3(\text{H}_2\text{O})_6[\text{Mo}(\text{CN})_7]_2 \cdot 6\text{H}_2\text{O}$. *Journal of the American Chemical Society*, **121**: 3349-3356.
- [17] Yeung, W.-F., Lau, P.-H., Lau, T.-C., Wei, H.-Y., Sun, H.-L., Gao, S., Chen, Z.-D., Wong, W.-T. (2005) Heterometallic M(II)Ru(III)₂ compounds constructed from trans-[Ru(salen)(CN)₂]⁻ and trans-[Ru(acac)₂(CN)₂]⁻. Synthesis, structures, magnetic properties, and density functional theoretical study. *Inorganic Chemistry*, **44**: 6579-6590.
- [18] Coronado, E., Galán-Mascarós, J.R., Gómez-García, C.J., Martínez-Agudo, J.M., Martínez-Ferrero, E., Waerenborgh, J.C., Almeida, M. (2001) Layered molecule-based magnets formed by decamethylmetallocenium cations and two-dimensional bimetallic complexes $[\text{M}(\text{II})\text{Ru}(\text{III})(\text{ox})_3]^-$ (M(II) = Mn, Fe, Co, Cu and Zn; ox = oxalate). *Journal of Solid State Chemistry*, **159**: 391-402.
- [19] Larionova, J., Mombelli, B., Sanchiz, J., Kahn, O. (1998) Magnetic properties of the two-dimensional bimetallic compounds $(\text{NBu}_4)[\text{M}(\text{II})\text{Ru}(\text{III})(\text{ox})_3]$ ($\text{NBu}_4 = \text{tetra-n-butylammonium}$; M = Mn, Fe, Cu; ox = oxalate). *Inorganic Chemistry*, **37**: 679-684.

- [20] Murray, K.S., Van den Bergen, A.M., West, B.O. (1978) Ruthenium complex with a tetradentate salicylaldimine Schiff base. *Australian Journal of Chemistry*, **31**: 203-207.
- [21] Leung, W.H., Che, C.M. (1989) Oxidation chemistry of ruthenium-salen complexes. *Inorganic Chemistry*, **28**: 4619-4622.
- [22] Bosnich, B., Tobe, M.L., Webb, G.A. (1965) Complexes of nickel(II) with a cyclic tetradentate secondary amine. *Inorganic Chemistry*, **4**: 1109-1112.
- [23] Yeung, W.-F., Man, W.-L., Wong, W.-T., Lau, T.-C., Gao, S. (2001) Ferromagnetic ordering in a diamond-like cyano-bridged Mn(II)Ru(III) bimetallic coordination polymer. *Angewandte Chemie, International Edition in English*, **40**: 3031-3033.
- [24] Figgis, B.N., Reynolds, P.A., Murray, K.S., Moubaraki, B. (1998) The ground state in tris(acetylacetonato)ruthenium(III) from low-temperature single-crystal magnetic properties. *Australian Journal of Chemistry*, **51**: 229-234.
- [25] Sheldrick, G.M. (1997): SHELXS-97, Program for Crystal Structure Determination. University of Göttingen, Germany.
- [26] Sheldrick, G.M. (1997): SHELXL-97, Program for the Refinement of Crystal Structures. University of Göttingen, Germany.